Research Paper

Activation of the mechanosensitive Ca^{2+} channel TRPV4 induces endothelial barrier permeability via the disruption of mitochondrial bioenergetics

Qing Lu [a], Evgeny A. Zemskov [a], Xutong Sun [a], Hui Wang [a,b], Manivannan Yegambaram [a], Xiaomin Wu [a], Alejandro Garcia-Flores [a], Shanshan Song [a], Haiyang Tang [a,b], Archana Kangath [a], Gabriela Zubiate Cabanillas [a,c], Jason X.-J. Yuan [d], Ting Wang [e], Jeffrey R. Fineman [f,g], Stephen M. Black [a,*]

[a] Department of Medicine, Division of Translational & Regenerative Medicine, University of Arizona, Tucson, AZ, USA
[b] College of Veterinary Medicine, Northwest A&F University, Yangling, Shaanxi, China
[c] Department of Chemist-Biological Sciences, Universidad de Sonora, Hermosillo, SON, Mexico
[d] Department of Medicine, University of California, San Diego, CA, USA
[e] Department of Internal Medicine, The University of Arizona Health Sciences, Phoenix, AZ, USA
[f] Department of Pediatrics, University of California San Francisco, San Francisco, CA, USA
[g] Cardiovascular Research Institute, University of California San Francisco, San Francisco, CA, USA

ARTICLE INFO

ABSTRACT

Mechanical ventilation is a life-saving intervention in critically ill patients with respiratory failure due to acute respiratory distress syndrome (ARDS), a refractory lung disease with an unacceptable high mortality rate. Paradoxically, mechanical ventilation also creates excessive mechanical stress that directly augments lung injury, a syndrome known as ventilator-induced lung injury (VILI). The specific mechanisms involved in VILI-induced pulmonary capillary leakage, a key pathologic feature of VILI are still far from resolved. The mechanoreceptor, transient receptor potential cation channel subfamily V member 4, TRPV4 plays a key role in the development of VILI through unresolved mechanism. Endothelial nitric oxide synthase (eNOS) uncoupling plays an important role in sepsis-mediated ARDS so in this study we investigated whether there is a role for eNOS uncoupling in the barrier disruption associated with TRPV4 activation during VILI. Our data indicate that the TRPV4 agonist, 4α-Phorbol 12,13-didecanoate (4αPDD) induces pulmonary arterial endothelial cell (EC) barrier disruption through the disruption of mitochondrial bioenergetics. Mechanistically, this occurs via the mitochondrial redistribution of uncoupled eNOS secondary to a PKC-dependent phosphorylation of eNOS at Threonine 495 (T495). A specific decoy peptide to prevent T495 phosphorylation reduced eNOS uncoupling and mitochondrial redistribution and preserved PAEC barrier function under 4αPDD challenge. Further, our eNOS decoy peptide was able to preserve lung vascular integrity in a mouse model of VILI. Thus, we have revealed a functional link between TRPV4 activation, PKC-dependent eNOS phosphorylation at T495, and EC barrier permeability. Reducing pT495-eNOS could be a new therapeutic approach for the prevention of VILI.

1. Introduction

Mechanical ventilation is a life-saving intervention in critically ill patients with respiratory failure due to acute respiratory distress syndrome (ARDS), a refractory lung disease with an unacceptable high mortality (30–50%) [1,2]. Paradoxically, mechanical ventilation also creates excessive mechanical stress that directly augments lung injury, a syndrome known as ventilator-induced lung injury (VILI) [1–4]. The deleterious synergy between excessive mechanical ventilation and ARDS, with a mortality of 30–40%, was underscored by the landmark ARDSnet trial [5] with ARDS survival negatively influenced by mechanical ventilation-generated mechanical stress [1–3]. VILI may also

---

occur in mechanically-ventilated patients even when ARDS is not initially present [6] and shares pathobiologic features with ARDS including increased nuclear factor (NF)-κB -dependent inflammatory cytokine expression and marked lung endothelial cell (EC) protein leakage [7–12]. Unfortunately, specific mechanisms involved in the development of VILI remain elusive highlighting the need for a more thorough understanding of VILI pathobiology and development of novel therapeutic targets and strategies.

A number of molecular mechanisms have been identified in VILI including Ca^{2+} dependent pathways, activation of protein kinases (including PKC and Rho kinase) and the modulation of eNOS activity [13], and an excessive ROS generation [14–17]. Interestingly, our recent study demonstrated that PKC-dependent phosphorylation of eNOS T495 leads to enzyme uncoupling, increased peroxynitrite production, and barrier disruption [18]. Further investigations also revealed that PKC dependent phosphorylation of eNOS at Thr495, increased mitochondrial derived ROS [19]. It is widely accepted that calcium entry into EC is necessary for barrier disruption [14]. As eNOS uncoupling can be catalyzed by PKCα [16] this suggest a link between increases in intracellular $[Ca^{2+}]$ and eNOS uncoupling and the EC barrier permeability associated with VILI. The TRP family has emerged as a predominant regulator of Ca^{2+} entry in endothelial cells [20]. Moreover, TRPV4 channels are abundantly expressed in lung microvascular endothelial cells [21] and the TRPV4 agonist, 4αPDD has been shown to cause EC injury [21]. Conversely, TRPV4 inhibition has been shown to attenuate both pulmonary barrier permeability and pro-inflammatory cytokine release during VILI [22]. TRPV4 dependent Ca^{2+} influx has also been shown to activate PKCα in EC [23]. Thus, the purpose of this study was to investigate if there is a mechanistic link between TRPV4 activation and eNOS uncoupling in the EC barrier permeability associated with VILI.

Using the agonist 4αPDD, our data confirm a mechanistic link between TRPV4 activation and the Ca^{2+}-activated PKC-dependent phosphorylation of eNOS at T495 that results in eNOS uncoupling, increased peroxynitrite production, and EC barrier disruption. Further, we demonstrate that PKC-dependent eNOS phosphorylation at T495 induced mitochondrial redistribution of eNOS and this correlated with a disruption of mitochondrial bioenergetics and increased mitochondrial ROS generation. The administration of eNOS decoy peptide designed to prevent phosphorylation of eNOS at T495 blocks TRPV4-induced eNOS mitochondrial redistribution, reduces mitochondrial ROS levels and preserves EC barrier function both in cultured PAEC and a mouse model of VILI.

2. Materials and methods

2.1. Cell culture

Primary cultures of ovine pulmonary arterial endothelial cells (PAEC) were isolated as described previously [24]. Briefly, cells were maintained in Dulbecco's modified Eagle medium (DMEM) supplemented with 10% fetal calf serum (Hyclone, Logan, UT), antibiotics/antimycotic (500 IU Penicillin, 500 μg/ml Streptomycin, 1.25 μg/ml Amphotericin B; MediaTech, Herndon, VA) at 37 °C in a humidified atmosphere with 5% CO_2 and 95% air. Cells were used for experiments between passages 9–14, seeded at ~50% confluence, and utilized when fully confluent.

2.2. Mouse model of VILI

Male C57BL/6 mice aged between 6 and 8 weeks were purchased from Jackson Laboratories (ME, USA). Mice were maintained at a room temperature of 22 ± 1 °C in air with 40–70% humidity at least one week before experiments. Animals were randomly distributed into 4 groups (n = 5 in each group): non-ventilated control mice with normal saline; non-ventilated control mice treated with the eNOS decoy peptide (d-

peptide); high tidal volume with normal saline; high tidal volume with eNOS decoy peptide. Three hours before ventilation, saline or the eNOS decoy peptide (10 mg/kg body weight) were injected intraperitoneally. Before mechanical ventilation was initiated, mice were anesthetized using an intraperitoneal injection with a cocktail containing ketamine (100 mg/kg) and xylazine (5 mg/kg). The mice were then placed in a supine position on a heating pad to maintain body temperature. For the ventilation procedure, mice were orotracheally intubated with a 20 g intravenous indwelling catheter and attached to a small animal ventilator (SAR-1000, CWE Inc., USA). The ventilation parameters were set as follows: inspiration/expiration ratio, 33%; respiratory rate, 75 breaths/min; and tidal volume, 35 mL/kg (high tidal volume group). During mechanical ventilation, mice were maintained in deep anesthesia by injecting with ketamine (100 mg/kg) every 45 min for the duration of the 4 h study. Mice in the non-ventilated control group were allowed to spontaneously breathe. At the end of the study period, 1 ml of prechilled PBS was used to flush the lungs through the tracheal cannula and the resulting bronchial alveolar lavage fluid (BALF) was collected and centrifuged at $500{\times}g$ for 10 min at 4 °C. The pellets were then resuspended in 500 μl of PBS and the cell numbers present were determined using an automated cell counter. The BAL fluid was centrifuged again at $15,000{\times}g$ at 4 °C for 15min and the supernatant collected and stored at −80 °C until the protein concentration was measured. After BALF collection, the mice were sacrificed immediately, and lungs were collected and frozen in liquid nitrogen for Western blot analysis. All animal procedures were approved by the Animal Care and Use Committee of the University of Arizona.

2.3. Immunohistochemical analysis of the mouse lung

Lungs were instilled with 10% formalin under 15 cmH$_2$O pressure and immersed in the same solution before tissue processing into paraffin-embedded blocks; 4 μm sections were then cut and stained with hematoxylin and eosin (H & E) as described previously [25,26].

2.4. Antibodies and chemicals

Mouse eNOS antibody, BD Transduction laboratories (San Jose, CA), Cat# 610296. Mouse eNOS (pT495) antibody, BD Transduction laboratories (San Jose, CA), Cat# 612706. Mouse β-actin antibody, Sigma (St. Louis, MO), Cat# A1978-200UL. Rabbit PKCα antibody, rabbit Phospho-(Ser) PKC antibody, Cell Signaling (Danvers, MA), Cat# 2056S. Mouse eNOS polyclonal antibody, ThermoFisher (Waltham, MA), Cat# PA3-031A. VE-Cadherin antibody, Millipore (Temecula, CA). Mito-Tracker, Invitrogen (Carlsbad, CA), Cat# 7512. MitoSOX Red, Molecular Probes (Eugene, OR). TMRM (tetramethylrhodamine methyl ester perchlorate), Molecular Probes (Eugene, OR), Cat# I34361. NucBlue Live Cell Staining, Invitrogen (Carlsbad, CA), Cat#R37605. Dihydrorhodamine 123, EMD Millipore (Billerica, MA), Cat# D1054. Goat Anti-Mouse/Rabbit Cy2 antibody and Goat Anti-Mouse/Rabbit Cy3 antibody, Jackson ImmunoResearch (West Grove, PA). 4αPDD (4α-Phorbol-12,13 didecanoate), Millipore (Billerica MA), Cat# 524394-1 MG. PMA (Phorbol 12-myristate 13-acetate), Sigma-Aldrich (St. Louis, MO), Cat# P1585.

2.5. Measurement of cytosolic Ca^{2+} concentration ($[Ca^{2+}]_{cyt}$)

PAEC were grown at 50–60% confluence on 25-mm-diameter circular glass coverslips. Cells were first incubated with 4 μM fura-2 acetoxymethyl ester (fura-2/AM; Invitrogen/Molecular Probes, Eugene, OR) in HEPES-buffered solution for 60 min at room temperature (22–24 °C) and then superfused with the HEPES-buffered solution for 30 min to washout residual extracellular fura-2/AM and allow sufficient time for intracellular esterase to cleave AM from fura-2/AM. Cells loaded with fura-2 were alternatively illuminated at 340 and 380 nm wavelengths by a xenon lamp (Hamamatsu Photonics, Hamamatsu,

Japan) connected to an inverted fluorescent microscope (Eclipse Ti-E; Nikon, Tokyo, Japan). The fluorescence emission (at 520 nm) was captured with an EM-CC camera (Evolve; Photometric, Tucson, AZ) and analyzed using NIS Elements 3.2 software (Nikon). $[Ca^{2+}]_{cyt}$ is expressed as 340/380 fluorescence ratio within an area of interest in the peripheral area of a cell recorded every 2 s. The 340/380 ratio was used to calculate the $[Ca^{2+}]_{cyt}$ in nanomolar concentration. $[Ca^{2+}]_{cyt}$ was calculated using the following equation: $[Ca^{2+}]_{cyt} = K_d \times (S_{f2}/S_{f1}) \times (R-R_{min})/(R_{max}-R)$. K_d (225 nM) is the dissociation constant of the Ca^{2+}-fura-2 complex; and S_{f2} and S_{f1} and R_{min} and R_{max} were calculated using a standard protocol [27]. The HEPES-buffered solution contained (in mM) 137 NaCl, 5.9 KCl, 1.8 $CaCl_2$, 1.2 $MgCl_2$, 14 glucose, and 10 HEPES (pH was adjusted to 7.4 with 10 N NaOH). The Ca^{2+}-free solution was prepared by replacing 1.8 mM $CaCl_2$ with equimolar $MgCl_2$ and adding 0.1 mM EGTA to chelate residual Ca^{2+}. All experiments for measurement of $[Ca^{2+}]_{cyt}$ were carried out at room temperature (22–24 °C).

2.6. Measurement of eNOS derived superoxide

Superoxide levels were estimated by electron paramagnetic resonance (EPR) assay using the spin-trap compound 1-hydroxy-3-methoxy-carbonyl-2,2,5,5-tetramethylpyrrolidine HCl (CMH, Axxora) as described previously [18,19]. Superoxide in PAEC was trapped by incubating PAEC with 20 μl of CMH stock solution (20 mg/ml) for 1 h, followed by trypsinization and centrifugation at 500*g*. The cell pellet was suspended in 35 μl DPBS and loaded into a capillary tube which was then analyzed with a MiniScope MS200 EPR machine (Magnettech, Berlin, Germany). Pre-incubating cells or tissue with 100 μM ethyl-isothiourea (ETU, Sigma-Aldrich) for 30 min followed by incubation with CMH measured NOS-derived superoxide. EPR spectra were analyzed using ANALYSIS v.2.02 software (Magnettech). Differences between levels of samples incubated in the presence and absence of ETU were used to determine NOS-dependent superoxide generation.

2.7. Determination of mitochondrial reactive oxygen species (ROS) levels

MitoSOX™ Red (Molecular Probes), a fluorogenic dye for selective detection of ROS levels in the mitochondria of live cells was used. Briefly, cells were washed with fresh media, and then incubated in media containing MitoSOX Red (2 μM), for 30 min at 37 °C in dark conditions then subjected to fluorescence microscopy at an excitation of 510 nm and an emission at 580 nm. An Olympus IX51 microscope equipped with a CCD camera (Hamamatsu Photonics) was used for acquisition of fluorescent images. The average fluorescent intensities (to correct for differences in cell number) were quantified using ImagePro Plus version 5.0 imaging software (Media Cybernetics, Rockville, MD).

2.8. Measurement of peroxynitrite levels

The level of cell peroxynitrite was determined by the oxidation of dihydrorhodamine (DHR) 123 (EMD Millipore, Billerica, MA) to rhodamine 123, as we have described [28]. Briefly, cultured PAEC were treated with or without TGF- β1 (5 ng/ml, 8 h) or GW9662 (5 μM, 24 h). Collect the cells and cell pellet were then treated with PEG-Catalase (100U, 30min) to reduce H_2O_2 dependent DHR 123 oxidation. DHR 123 (5 μM, 30min) was added to the cell pellet in phenol red-free media and the fluorescence of rhodamine 123 measured using a Fluoroskan Ascent Microplate Fluorometer with excitation at 485 nm and emission at 545 nm. Fluorescent values were normalized to the protein levels in each sample.

2.9. Analysis of mitochondrial membrane potential

Mitochondrial membrane potential was determined using TMRM (tetramethylrhodamine methyl ester perchlorate, Molecular Probes,

Eugene, OR). Briefly, after each experiment, cells were washed with fresh media, incubated in media containing TMRM (50 nM), for 30 min at 37 °C in dark conditions, then subjected to fluorescence microscopy using an excitation of 548 nm and an emission at 575 nm. An Olympus IX51 microscope equipped with a CCD camera (Hamamatsu Photonics) was used for acquisition of fluorescent images and the average fluorescent intensities were quantified using ImagePro Plus version 5.0 imaging software (Media Cybernetics).

2.10. Analysis of mitochondrial bioenergetics

The XF24 Analyzer (Seahorse Biosciences) and XF Cell Mito Stress Test Kit (# 101706–100; Seahorse Biosciences) were used for the mitochondrial bioenergetic analyses. The optimum number of cells/well was determined to be 75,000/0.32 cm^2. At the end of each study, The XF24 culture microplates were incubated in a CO_2-free XF prep station at 37 °C for 45 min to allow temperature and pH calibration. Subsequently each well was sequentially injected Oligomycin (1 μM final concentration), carbonyl cyanide 4-(trifluoromethoxy) phenylhydrazone (FCCP, 1 μM final concentration), and Rotenone + antimycin A (1 μM final concentration of each) and measured the oxygen consumption rate (OCR). Using these agents, we determined basal mitochondrial respiration, reserve respiratory capacity and maximal respiratory capacity measurements in pmols/min of oxygen consumed.

2.11. Western blot analysis

Protein extracts were prepared using lysis buffer (50 mM Tris-HCl, pH 7.6, 0.5%Triton X-100, 20% glycerol) containing Halt™ protease inhibitor cocktail (Pierce Laboratories, Rockford, IL). The extracts were then subjected to centrifugation (15,000 g for 15 min at 4 °C). Supernatant fractions were assayed for protein concentration using the Bradford reagent (Bio-Rad, Richmond, CA) then used for Western blot analyses. Protein extracts (25–50 μg) were separated on Long-Life 4–20% Tris-SDS-Hepes gels and electrophoretically transferred to Immuno-Blot™ PVDF membrane (Bio-Rad Laboratories, Hercules, CA). Immunoblotting was then carried out using the appropriate antibodies in Tris-base buffered saline with 0.1% Tween 20 and 5% nonfat milk. After washing, the membranes were probed with horseradish peroxidase-conjugated goat antiserum to rabbit or mouse. Reactive bands were visualized using chemiluminescence (Super Signal West Femto; Pierce, Rockford, IL) on a LI-COR Odyssey image station (Lincoln, NE). Bands were quantified using LI-COR Image Station software. Loading was normalized by reprobing the membranes with an antibody specific to β-actin.

2.12. Immunofluorescent microscopy

PAEC were grown on cover glass for three days after reaching 100% confluence, and fixed with 4% paraformaldehyde (Thermo Fisher Scientific) for 30 min, permeabilized with 100% cold methanol at −20 °C for 5 min. Cell then blocked with 1% BSA for 1 h, and later incubated with first antibody overnight at 4 °C then secondary antibody at room temperature for 1 h. Finally, cells were mounted on microscope slides using ProLong Glass Antifade Mountant, (Invitrogen, Carlsbad, CA, Cat# P36980). Immunofluorescent images were observed with a Nikon Eclipse TE2000-U microscope, with Hamamatsu digital camera C11440, and Olympus IX51 microscope with Hamamatsu digital camera C4742-95. The images were analyzed with ImagePro Plus 7.0 [29] or ImageJ software to evaluate the colocalization of fluorescent.

2.13. Measurement of PKC activity

Activation of PKC in control and 4αPDD-treated EC was evaluated using dot-blot method and antibodies specific to PKC-phosphorylated proteins. The cell lysates were transferred on nitrocellulose membrane

using Bio-Dot Microfiltration apparatus (Bio-Rad) according to Instruction Manual. To detect and evaluate levels of PKC-phosphorylated proteins, Phospho-(Ser) PKC Substrate rabbit polyclonal antibody (Cell Signaling) was used. After visualization of PKC-phosphorylated proteins, the membrane was stripped and re-probed with β-actin antibody for normalization.

2.14. Transient transfections

The constitutively active PKCα mutant, myr-PKCα was purchased from Origene (Rockville, MD) and purified using an endotoxin free kit (Qiagen, USA). PAEC cultured to 80% confluence were then transiently transfected using the Effectene Transfection Reagent (Qiagen, USA) according the manufacturers protocol.

2.15. In vitro peptide binding assay

The T495-eNOS decoy (d)-peptide was synthesized commercially by PEPTIDE 2.0 Inc. (Chantilly, VA). Biotinylation of the d-peptide was performed using the Thermo Scientific EZ-Link Sulfo–NHS–LC-Biotinylation Kit. Briefly, Sulfo–NHS–LC-Biotin was mixed with d-peptide and the reaction mix was incubated at room temperature for 30 min. Different concentrations of the biotinylated d-peptide (0–5 μg) mixed with either purified eNOS protein or PKCα protein in a reaction mix containing PKC lipid activator were incubated at room temperature for 1 h. Protein bound to the biotinylated d-peptide was captured using Thermo Scientific streptavidin agarose column and run on a 10% SDS-PAGE gel under reducing condition. The resulting blots were probed with antibodies to eNOS and PKCα protein respectively. Reactive bands were visualized using chemiluminescence on the LI-COR Odyssey image station.

2.16. Measurement of trans endothelial resistance (TER)

Transendothelial Electrical Resistance (TER) was determined to characterize the integrity of PAEC monolayers using an electrical cell-substrate impedance sensing (ECIS) instrument ECIS Z-Theta (Applied BioPhysics, Troy, NY) as previously described [30,31] The cells were plated in 8-well ECIS arrays (Applied BioPhysics) in complete cell culture medium (DMEM supplemented with 10%-FBS) and grown to 100%-confluency for 2 days. Then, cell culture medium was changed for fresh one, and the EC were used in TER assay. Initial resistance at the onset of our experiments was 900–1000 in array wells, and then all wells were normalized to 1.4000-Hz AC signal with 1-V amplitude was applied to the EC monolayers through a 1-M-Ω resistor, creating an approximate constant-current source (1 μA). After a baseline measurement, the EC were treated with 4αPDD, PMA, the eNOS pT495 decoy peptide, or vehicle at the concentrations described in Figure Legends, and changes in TER were recorded in real time.

2.17. Statistical analysis

Statistical calculations were performed using the GrapPad Prism software. The mean ± SEM was calculated for all samples. Statistical significance was determined either by the unpaired t-test (for 2 groups) or ANOVA (for $\geq$3 groups) with Newman-Keuls post-hoc testing. A value of $P < 0.05$ was considered significant.

3. Results

3.1. The increase in permeability induced by the TRPV4 agonist, 4αPDD is associated with the disruption of mitochondrial function in pulmonary arterial endothelial cells

$[Ca^{2+}]_{cyt}$ measurements were performed with fura-2/AM loaded PAEC to confirm that 4αPDD exposure induces a transient increase of $[Ca^{2+}]_{cyt}$ via Ca^{2+} influx (Fig. 1 A&B). The increase in $[Ca^{2+}]_{cyt}$ correlates with a dose-dependent decrease in TER, indicating a disruption of barrier integrity (Fig. 1C). The decrease in TER induced by TRPV4 activation correlates with the disruption of mitochondrial function as determined by increases in mitochondrial ROS levels, estimated by increases in MitoSOX red fluorescence (Fig. 2A) and a decrease in the mitochondrial membrane potential, evaluated using the probe tetramethylrhodamine methyl ester (TMRM, Fig. 2A). We also measured effects on mitochondrial bioenergetics (Fig. 2B). Our data indicate that 4αPDD disrupts bioenergetics as determined by reductions in mitochondrial basal O_2 consumption, spare respiratory capacity and maximum respiratory capacity (Fig. 2C).

3.2. The 4αPDD-mediated disruption of mitochondrial bioenergetics is associated with the mitochondrial redistribution of uncoupled eNOS in pulmonary arterial endothelial cells

We have previously shown that phosphorylation of eNOS at T495 by PKC results in its uncoupling and mitochondrial redistribution [19]. Thus, we next investigated if this was the mechanism by which TRPV4 activation disrupts mitochondrial function. Our data indicate that the increase in intracellular $[Ca^{2+}]$ associated with 4αPDD exposure (Fig. 1A) increases PKC activity in PAEC (Fig. 3A). This results in an increase in eNOS phosphorylation at T495 (Fig. 3B) and eNOS uncoupling as determined by increases in NOS derived superoxide generation (Fig. 3C) and cellular peroxynitrite levels (Fig. 3D). Immunofluorescence microscopy confirmed that 4αPDD exposure induces the mitochondrial redistribution of eNOS (Fig. 3E&F). Further, we found that cyclic stretch mimicked the effect of 4αPDD in PAEC, increasing both pT495-eNOS levels (Fig. 3G) and the mitochondrial redistribution of eNOS (Fig. 3H). As laminar shear stress did not increase either pT495-eNOS levels (Fig. 3I) or the mitochondrial redistribution of eNOS (Fig. 3I) these data demonstrate differential effects of mechanical forces on eNOS phosphorylation and sub-cellular redistribution.

To confirm the role of PKC in the phosphorylation of eNOS at T495 and the disruption of mitochondrial function we next exposed PAEC to the PKC activator, phorbol myristate acetate (PMA). PMA was able to mimic the effects of 4αPDD as we could identify increases in pT95-eNOS levels (Fig. 4A), eNOS uncoupling (Fig. 4B), and the disruption of mitochondrial bioenergetics (Fig. 4C&D). PMA exposure also induced the mitochondrial redistribution of eNOS (Fig. 4 E&F). More specifically, the over-expression of a constitutively active mutant of PKCα alone (Fig. 5A) was able to recapitulate the action of 4αPDD stimulating eNOS phosphorylation at T495 (Fig. 5B), eNOS uncoupling (Fig. 5C) while increasing mitochondrial ROS levels (Fig. 5D) and decreasing the mitochondrial membrane potential (Fig. 5E). Mitochondrial bioenergetics were also disrupted (Figure F&G) and the mitochondrial redistribution of eNOS was increased (Fig. 5G).

3.3. Blocking eNOS phosphorylation at T495 attenuates the injury associated with mechanical ventilation of the mouse lung

To further investigate the role of eNOS phosphorylation at T495 in the increase in permeability induced by TRPV4 activation we developed a decoy peptide (d-peptide) designed to prevent eNOS T495 phosphorylation. The peptide, sequence HRKKRRQRRITRKKTFKEVA, was first tested for specificity using an *in vitro* binding assay. Our data indicate that the d-peptide is able to bind efficiently to purified PKCα (Fig. 6A) but not to eNOS (Fig. 6A) indicating it acts as a decoy of eNOS for PKC. When introduced into PAEC, the d-peptide attenuates the PMA-mediated increase in pT495-eNOS (Fig. 6B) and reduces eNOS uncoupling (Fig. 6C). The PMA-induced mitochondrial redistribution of eNOS is attenuated (Figure D&E) and the barrier disruption induced by 4αPDD is reduced as determined by the preservation of TER (Fig. 6F) and VE-Cadherin mean fluorescence (Fig. 6G &H). The d-peptide attenuates the increase in pT495-eNOS induced by mechanical ventilation of the
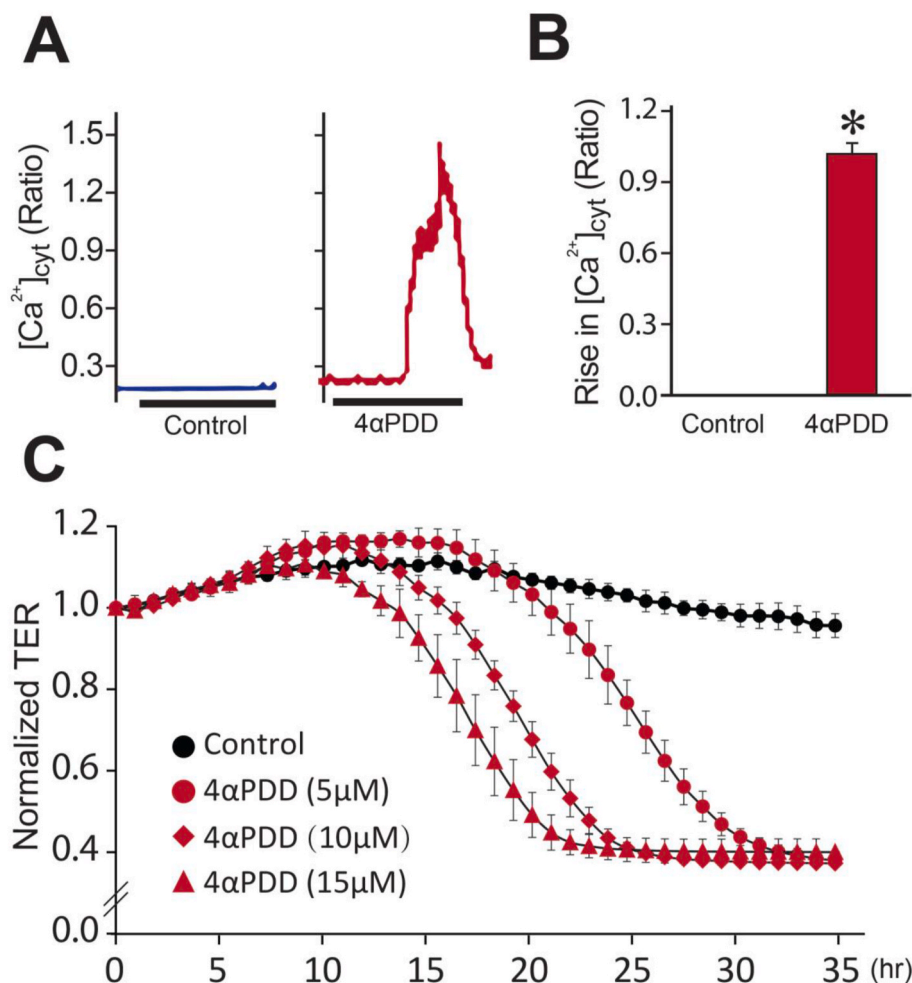
Fig. 1. TRPV4 activation disrupts the endothelial barrier in pulmonary arterial endothelial cells. The TRPV4 agonist, 4αPDD (10 μM) induces a transient increase in cytosolic free Ca^{2+} concentration ($[Ca^{2+}]_{cyt}$) in PAEC (A&B). 4αPDD (0–15 μM) also causes a dose-dependent decrease in normalized TER (C). Data are mean ± SEM. n = 3. *$P < 0.05$ vs. Control.
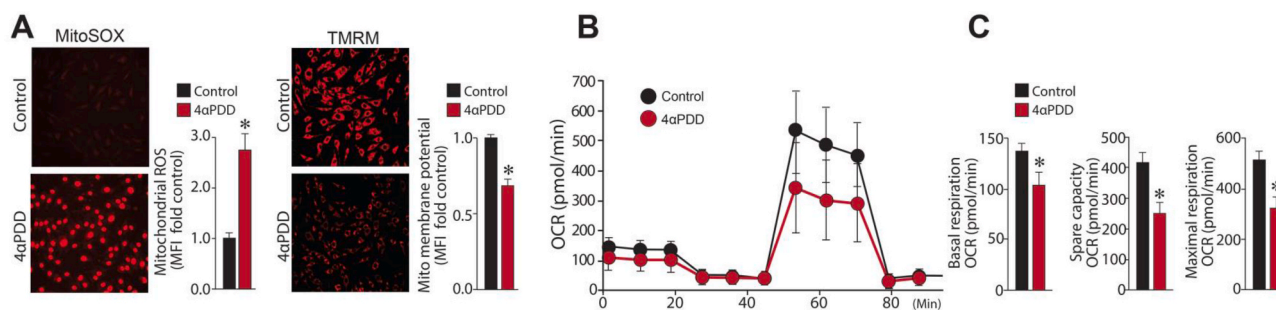

Fig. 2. TRPV4 activation disrupts mitochondrial bioenergetics in pulmonary arterial endothelial cells. Exposing PAEC to 4αPDD (10 μM, 3 h), increases mitochondrial reactive oxygen species (ROS) and reduces the mitochondrial membrane potential in PAEC, as determined by changes in mean fluorescence intensity (MFI) (A). 4αPDD also affects mitochondrial bioenergetics (B) with significant reductions in basal mitochondrial respiration, spare respiratory capacity, and maximal respiratory capacity (C). Values are mean ± SEM; n = 9–10. *$P < 0.05$ vs. Control.

mouse lung (Fig. 6I). This correlates with a reduction in VILI as demonstrated by decreases in the cell number (Fig. 6J), protein levels (Fig. 6K) in the BALF indicative of decreased pulmonary capillary permeability. H&E staining of mouse lung sections demonstrates a lung histopathology a typical of acute respiratory distress syndrome which includes atelectasis and thickened alveolar walls (shown by * in Fig. 6L) as well as alveolar edema and fibrin (shown by red arrows in Fig. 6L). We also identified evidence of vascular injury and perivascular edema

(shown by black arrows in Fig. 6L). These histopathologic features are reduced in the presence of the d-peptide (Fig. 6L).

4. Discussion

Ventilator-induced lung injury (VILI) is the consequence of acute lung injury (ALI) that occurs with the use of mechanical ventilation [32]. VILI is indistinguishable morphologically, physiologically, and
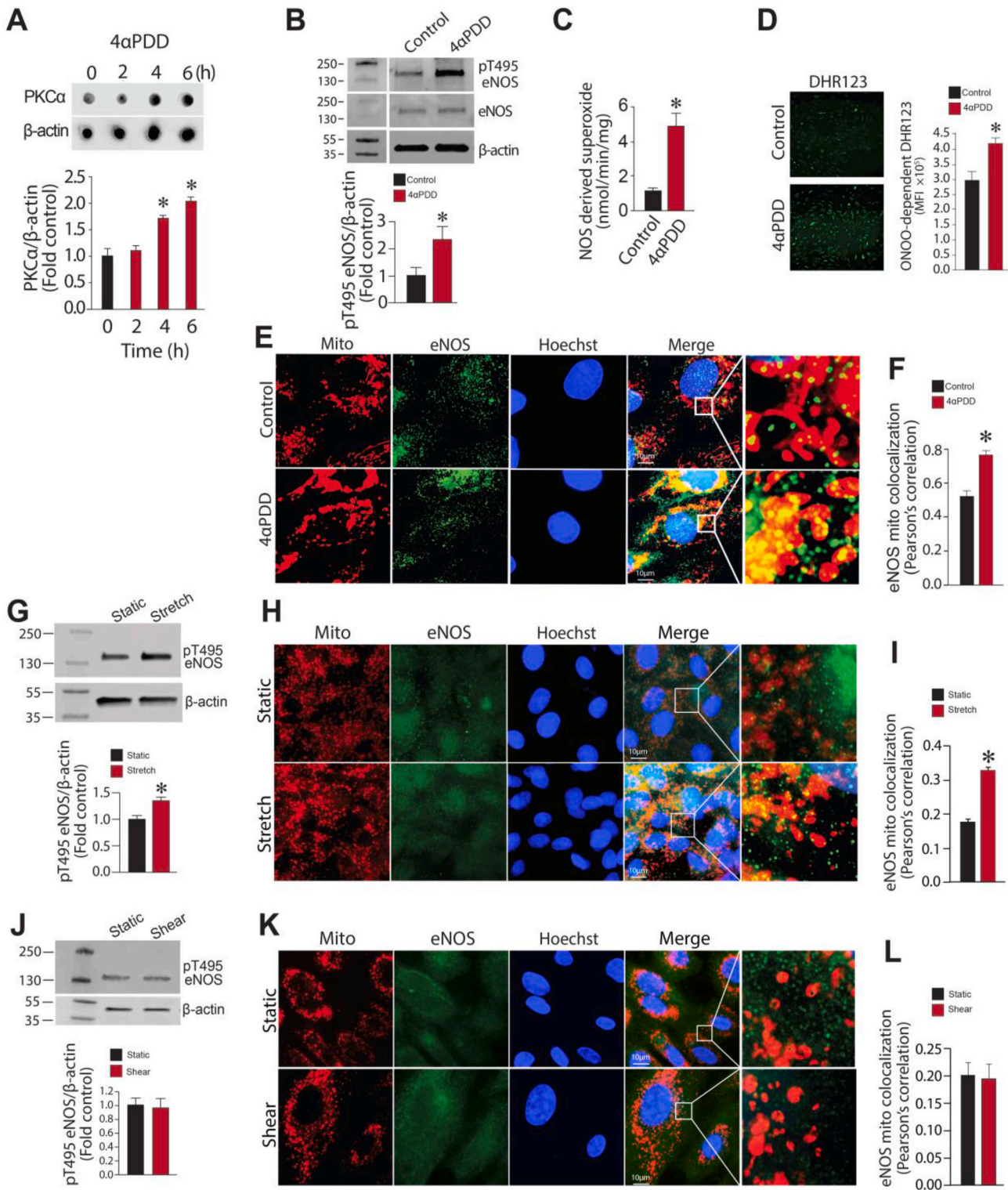
Fig. 3. TRPV4 activation induces the uncoupling and mitochondrial redistribution of eNOS in pulmonary arterial endothelial cells. Exposing PAEC to 4αPDD (10 μM) induces a time-dependent increase in PKC activity (A). eNOS phosphorylation at T495 is increased (B). eNOS derived superoxide (C) and cellular peroxynitrite levels (D) also increase. Immunofluorescence analysis shows that 4αPDD induces the mitochondrial redistribution of eNOS (E&F). Cyclic stretch (18% stretch, 1 Hz, 4 h) mimics the effect of 4αPDD with increases in pT495-eNOS levels (G) and the mitochondrial redistribution of eNOS (H&I). Neither pT495-eNOS (J) nor eNOS mitochondrial redistribution (K&L) are increased by laminar shear stress (20 dyn/cm², 4 h). Values are mean ± SEM; n = 3–10. *P < 0.05 vs. Control.

radiologically from the diffuse alveolar damage seen in ALI [32]. VILI is a significant problem with the use of mechanical ventilation to treat ARDS [32]. Mechanical ventilation itself can also injure the lungs even when ALI or ARDS is not initially present [6,33,34]. The current standard of patient for ALI/ARDS uses protective lung ventilation strategies [9,12,35]. These ventilator strategies are based on the ARDS network trial [36]. However, these protective ventilation strategies are supportive and not therapeutic. Thus, there is intense interest in
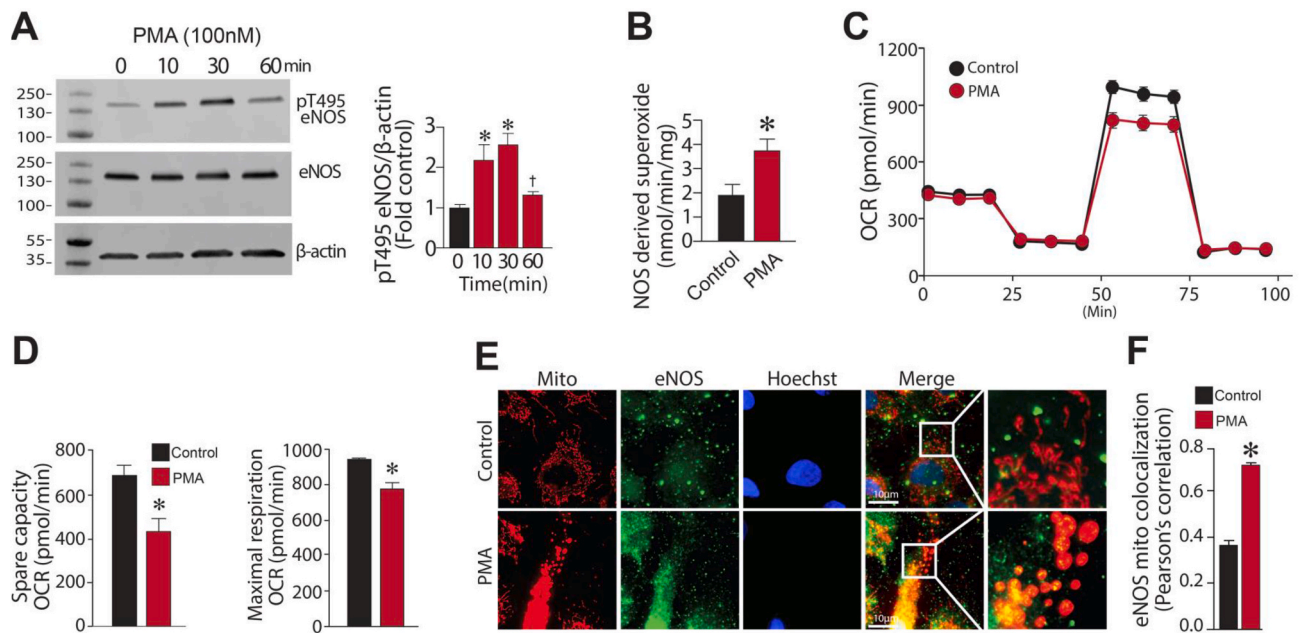
Fig. 4. PKC activation disrupts mitochondrial bioenergetics in pulmonary arterial endothelial cells. Exposing PAEC to the PKC activator, PMA (100 nM, 0–60min) induces a transient increase in pT495eNOS levels (A) and eNOS uncoupling (B). PMA also affects mitochondrial bioenergetics (C) with significant reductions in the spare- and maximal-respiratory capacities (D). Immunofluorescence analysis shows that PMA induces the mitochondrial redistribution of eNOS (E&F). Values are mean ± SEM; n = 3–10. *$P < 0.05$ vs. untreated. †$P < 0.05$ vs prior time point.

understanding the molecular mechanisms by which VILI leads to the development of ARDS. One of the major areas of investigation in VILI is the mechanical force dependent activation of transient receptor potential (TRP) channels which are permeable to Ca^{2+} since aberrant Ca^{2+} entry is one of the most widely acknowledged mechanisms that induce endothelial permeability [37,38]. In mammals, 28 TRP channel isoforms have been identified which are divided into six subfamilies, TRPA, TRPC, TRPM, TRPML, TRPP and TRPV. They present a common feature of a tetrameric structure, four subunits forming the pore of the channel and a ring of four negative charged residues at the external end of the pore composing the selectivity filter [39,40]. TRPV4 has been identified as a key Ca^{2+} channel [41] and is activated by physical stimuli such as mild heat, hypoosmotic conditions, and membrane deformation [42]. TRPV4 activation and Ca^{2+} entry can also occur by mechanical stimulation and our data show that the exposure of PAEC to cyclic stretch induces eNOS phosphorylation and eNOS mitochondrial redistribution in a similar manner to the direct activation of TRPV4 using 4α-phorbol didecanoate (4αPDD). Interestingly, the exposure of PAEC to laminar shear stress for the same duration did not induce eNOS phosphorylation or eNOS mitochondrial redistribution. This supports multiple prior work which has indicated that the endothelium responds differently depending on the mechanical force to which it is exposed. However, the literature is far from clear. Thus, mechanical stress has been shown to both uncouple eNOS [43] and stimulate NO generation [44] from eNOS. This is likely due to differential effects on ECs from different ages, vascular beds and potentially to both the duration and level of the mechanical force utilized [43,45–47]. In addition, although laminar shear stress predominantly stimulates eNOS activity and NO release [48–52], oscillatory flow uncouples eNOS [53]. Thus, different types of mechanical forces can act differently on regions of the vascular wall to affect NO bioavailability and potentially contribute to disease pathogenesis. We propose that this, at least acutely, could be dependent on which phosphorylation site on eNOS is regulated such that increasing pS1177-eNOS levels will be associated with eNOS activation and NO generation [54] while increases in pT495-eNOS will be associated with eNOS inactivation and uncoupling [18,19,55].

High vascular pressure and ventilator-induced lung injury have both

been reported to increase lung endothelial permeability by promoting Ca^{2+} entry via TRPV4 [56,57] and 4αPDD exposure also leads to Ca^{2+} entry-dependent acute lung injury, disruption of the lung barrier, and alveolar flooding [21]. Conversely, 4αPDD does not increase lung permeability in TRPV4-knockout mice [21]. However, beyond Ca^{2+}-mediated cytoskeleton rearrangements [58] the mechanisms by which TRPV4 activation induces EC permeability are unresolved. Thus, our results add significantly to our knowledge regarding TRPV4 mediated EC permeability by demonstrating an important role for PKC-mediated phosphorylation and uncoupling of eNOS in the development of VILI. Recent studies have demonstrated that $TRPV4^{-/-}$ mice or mice treated with the TRPV4 antagonist, GSK2193874 are protected against acid-induced ALI [59]. Interestingly, TRPV4 inhibition was only protective if given in a preventative manner [59]. This lack of a therapeutic window suggests that the downstream targets of TRPV4 may be more viable targets for therapy. Indeed, our data demonstrating that targeting eNOS phosphorylation at T495 using our decoy peptide attenuates VILI in a mouse model of mechanical stretch, validates this approach and potentially opens up a new avenue for treating/preventing VILI in humans. However, it is likely that our d-peptide will require significant modifications to increase its stability and also be linked with a delivery system that will specifically target the damaged endothelium before it will be ready for trials in human patients. This will require significant future investigations but it may prove worthwhile as it has been shown that ARDS cases stratified according to disease severity have been shown to be associated with VILI in 48.8% of the entire patient population, 87% in late ARDS, 46% in intermediate ARDS, and 30% in early ARDS [60].

Our identification of a role for eNOS uncoupling in TRPV4 mediated EC barrier disruption is in agreement with prior work that has shown that eNOS is an important source of ROS in VILI [43]. As eNOS uncoupling is associated with ALI in gram positive [18] and gram negative bacteria [61] exposure models as well a smoke inhalation and burn injury models [62] it is likely a common mechanism for the development of ALI induced by multiple stimuli. However, the mechanism by which eNOS becomes uncoupled can be different. Our data implicate T495 phosphorylation in eNOS uncoupling in VILI and gram positive sepsis
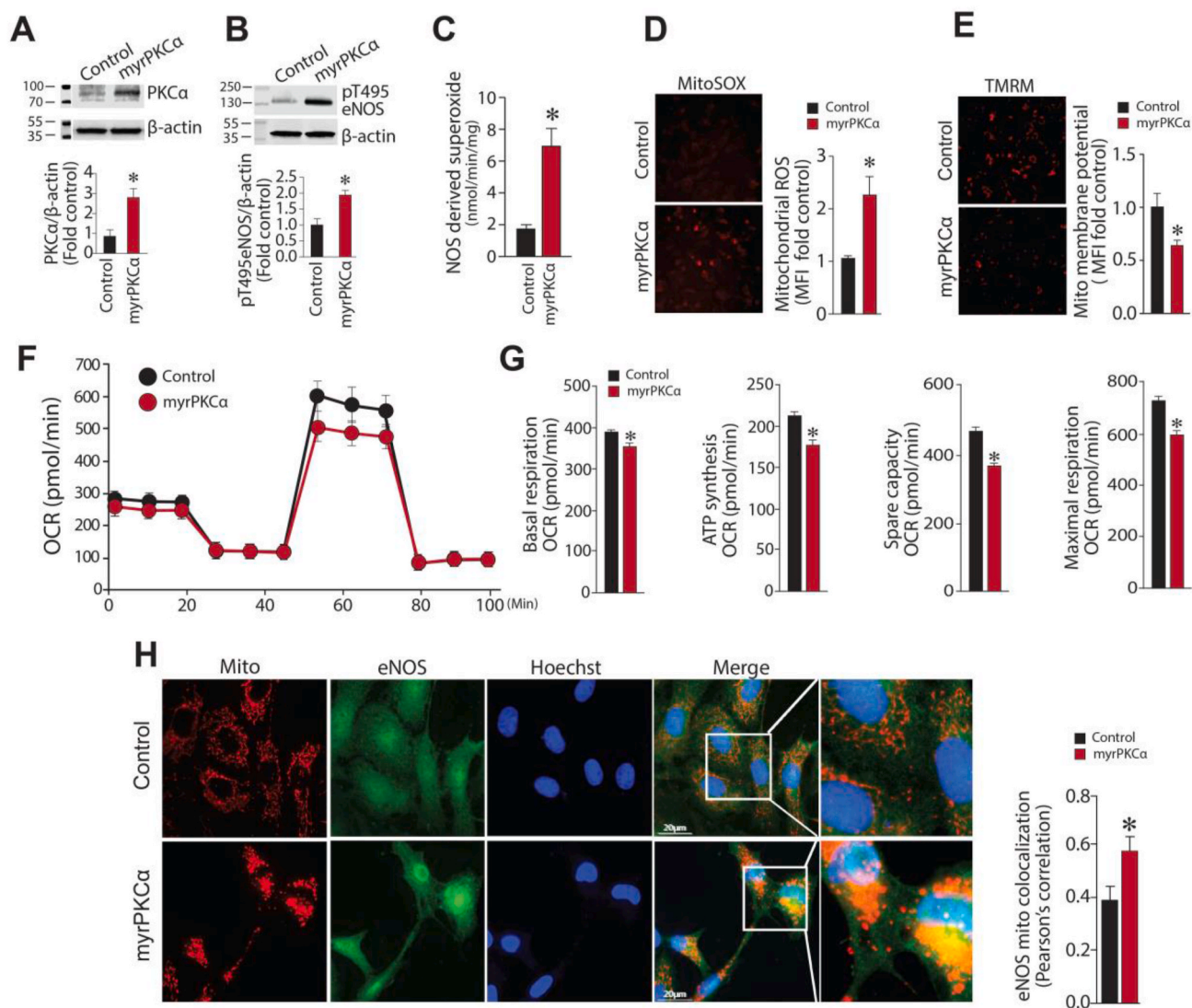
Fig. 5. The over-expression of a constitutively active PKCα mutant mimics the effects of TRPV4 activation in pulmonary arterial endothelial cells. PAEC were transiently transfected with a constitutively active PKCα mutant (Myr-PKCα) for 48 h. Myr-PKCα over-expression (A) increases pT495eNOS levels (B) and NOS-derived superoxide (C). Myr-PKCα over-expression also increases mitochondrial ROS (D) and reduces the mitochondrial membrane potential in PAEC (E). Mitochondrial bioenergetics are also disrupted (F) with significant reductions in basal mitochondrial respiration, O_2 consumed for ATP synthesis as well as the spare-, and maximal-respiratory capacity (G). Immunofluorescence analysis shows that Myr-PKCα over-expression induces the mitochondrial redistribution of eNOS (H). Values are mean ± SEM; n = 3–10. *$P < 0.05$ vs. untreated.

[18] while in gram negative sepsis-eNOS uncoupling involves increases in the levels of the endogenous NOS uncoupler, asymmetric dimethlyarginine (ADMA) [31,63]. A previous study has also shown that mechanical ventilation is associated with the oxidation of tetrahydrobiopterin (BH_4) to BH_2 [43] and important NOS co-factor that is required for efficient enzymatic coupling [64–66]. As we have shown that BH_2 itself can increase eNOS uncoupling [67] it is possible that increases in BH_2 could synergize with T495 phosphorylation to further increase eNOS uncoupling. However, future studies will be required to test this hypothesis.

We have also previously shown in pulmonary hypertension (PH) that an endothelin-1 (ET-1) mediated increase in PKCδ activity induces the mitochondrial redistribution of eNOS through increased phosphorylation of eNOS at T495 [19] and that increased peroxynitrite generation is a prerequisite for the mitochondrial redistribution of uncoupled eNOS [68]. As we show here that T495 phosphorylation induces eNOS uncoupling and peroxynitrite generation it is possible that the phosphorylation of T495 is a common mechanism by which kinases can stimulate the mitochondrial redistribution of eNOS. Indeed Rho-kinase

(ROCK) has been shown to phosphorylate eNOS at T495 [69] and is also intimately involved in the development of ALI [70] we speculate that ROCK signaling may also induce EC barrier disruption through increases in T495 phosphorylation. However, it should also be noted that the mitochondrial redistribution of eNOS can also be induced by its phosphorylation at S635 by Akt1 [68,71]. However, in this case eNOS appears to enhance mitochondrial function as a S635D-eNOS mutant reduces the mitochondrial OCR and reduces mitochondrial ROS levels [68]. As it is becoming more accepted that Akt1 is involved in the resolution phase of ALI [72] it is interesting to speculate that mitochondrial redistributed eNOS due to phosphorylation at S635 could reduce mitochondrial ROS and perhaps mitochondrial function. This could be important due to the key role played by mitochondrial ROS in the inflammatory response via the activation of the inflammasome. Although important for the clearance of pathogens during bacterial infection, sustained or excessive inflammasome activation may exacerbate pathological inflammation [73]. Inflammasomes are a group of cytosolic protein complexes that regulate the activation of caspase-1, and the processing of pro-interleukin (IL)-1ß and pro-IL-18 to their mature
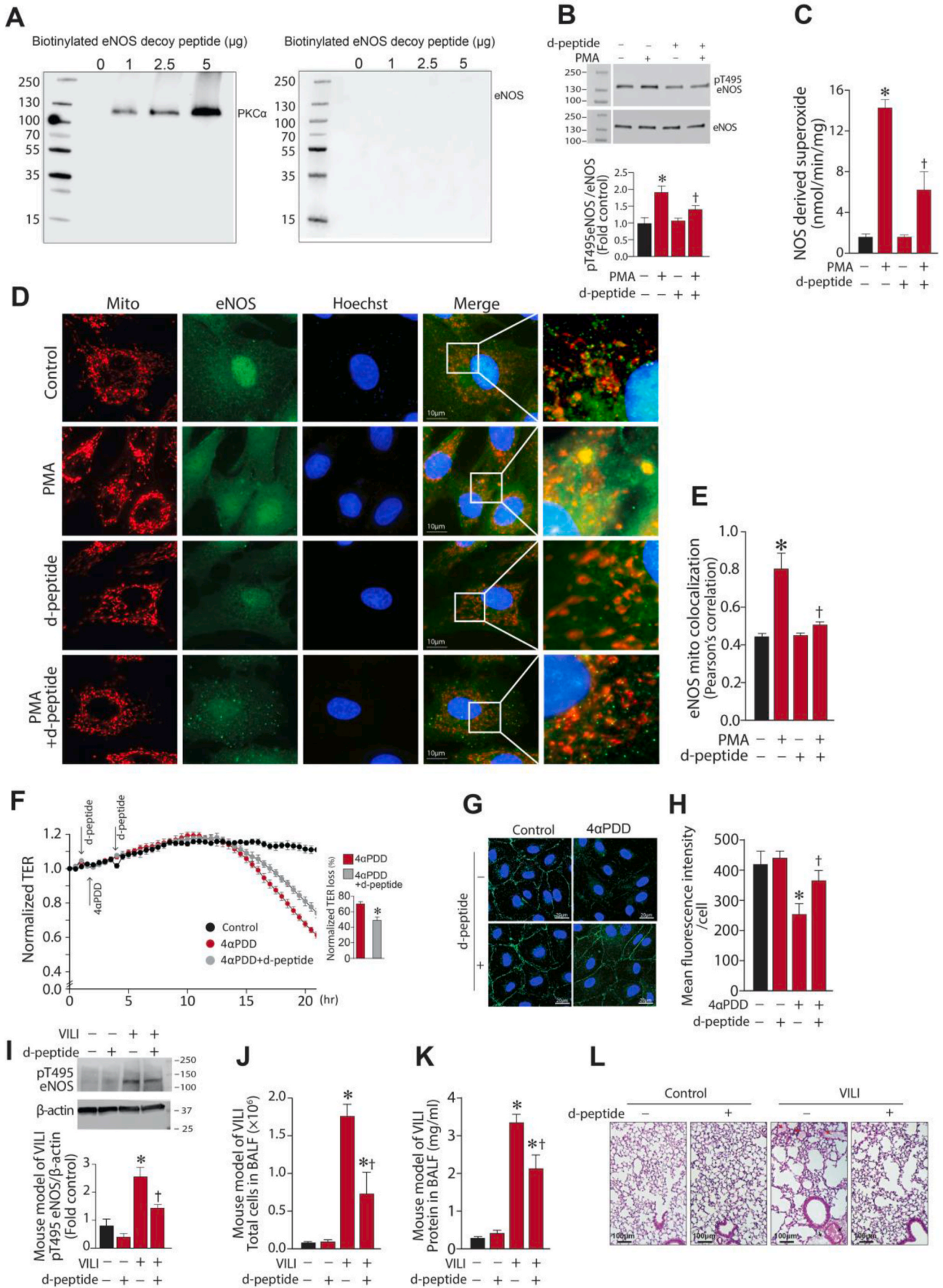
(caption on next page)

Fig. 6. Blocking eNOS phosphorylation at T495 attenuates endothelial barrier disruption <u>in vitro</u> and <u>in vivo</u>. The T495 eNOS decoy peptide (d-peptide) is able to bind efficiently to purified PKCα, but not eNOS (A). Treating PAEC with the d-peptide (1 μg/ml) attenuates the PMA (100 nm, 2 h)-mediated increase in pT495eNOS (B) and prevents the PMA-mediated increase in eNOS-derived superoxide (C). Immunofluorescence analysis shows that d-peptide attenuates the PMA-mediated mitochondrial redistribution of eNOS (D&E) and the 4αPDD (10 μM) dependent disruption of the EC barrier and endothelial junctional integrity as determined by ECIS (F) and VE-cadherin immunofluorescence staining (G&H). In the mouse model of VILI, the d-peptide decreases the stretch dependent increase in pT495eNOS (I) and attenuates the increase in capillary permeability as determined by reductions in the cell number (J) and protein concentration (K) in the BALF. H&E stained mouse lung sections (L) show that VILI causes atelectasis and thickened alveolar walls (*), alveolar edema and fibrin (red arrow), as well as vascular injury and evidence of perivascular edema (black arrow). The presence of the d-peptide prevents the development of these injurious events (L). Representative images are shown. Values are mean ± SEM; n = 3–10. *$P < 0.05$ vs. Control. †$P < 0.05$ vs PMA or VILI alone. (For interpretation of the references to colour in this figure legend, the reader is referred to the Web version of this article.)

active forms [74]. The activation of the NLRP3 inflammasome is a two-step process: the expression of NLRP3 and pro-IL-1ß is induced by transcriptional up-regulation via NF-κB signaling [75] followed by the assembly of NLRP3 inflammasome protein components in order to form a platform to activate caspase-1. Caspase 1 is then able to cleave pro-IL-1ß and pro-IL-18 allowing them to be secreted from cells [74]. As one of the mechanisms identified for NLRP3 inflammasome assembly is the generation of mitochondrial ROS [76], it likely that the mitochondrial redistribution of pT495-eNOS could be involved in the activation of the inflammasome while the mitochondrial redistribution of pS635-eNOS could be involved in the attenuation of inflammasome activity and the resolution of the inflammatory signal. This possibility is supported by data demonstrating that Akt1 is activated by protein nitration at Y^{350} in PAEC [68]. However, future studies will be required to investigate this possibility.

The downstream effector of mitochondrial redistributed uncoupled eNOS is likely peroxynitrite, formed from the interaction of NO with superoxide. It has been previously shown that peroxynitrite levels in the lung increase in response to mechanical ventilation [77,78]. However, the protein targets are far form resolved. Peroxynitrite introduces a covalent modification that adds a nitro group (-NO$_2$) to one ortho carbon of tyrosine's phenolic ring to form 3-nitrotyrosine (3-NT) in target proteins. Protein tyrosine nitration can signifcantly alter the structure-function of affected proteins due to the introduction of a net negative charge to the nitrated tyrosine at physiological pH, [79]. Although our study did not identify the protein targets responsible for the disruption of mitochondrial bioenergtics and the increase in mitochondrial ROS, it is likely that at least one of these is carnitine acetyl transferase (CrAT) an important member of the carnitine shuttle involved in fatty acid oxidation (FAO). This is based on our prior work which has identified CrAT as being susceptible to nitration mediated inhibition [80] and identified the disruption of carnitine homeostasis as having a key role in the development of pulmonary vascular disease [80–84]. In addition, impaired FAO has been shown to be involved in the development of ALI [85–87] and a pT495-eNOS mimic, T495D-eNOS induces CrAT nitration and disrupts carnitine homeostasis in PAEC [19]. However, future wok will be requied to clarify the role of FAO and carnitine homeostasis in the development of VILI.

In conclusion, our data establish a functional link between the activation of the mechanosensitive Ca^{2+} channel, TRPV4 and endothelial hyperpermeability through the phosphorylation and mitochondrial redistribution of eNOS mediated by PKC. Further, our studies using an eNOS decoy peptide suggest that targeting mitochondrial dependent redox pathways may have significant therapeutic value in the treatment of VILI in humans.

Declaration of competing interest

The authors have no conflict of interest to declare related to this research article.

Acknowledgements

References

[1] C.H. Goss, R.G. Brower, L.D. Hudson, G.D. Rubenfeld, Incidence of acute lung injury in the United States, Crit. Care Med. 31 (6) (2003) 1607–1611.

[2] M.A. Matthay, G.A. Zimmerman, C. Esmon, J. Bhattacharya, B. Coller, C. M. Doerschuk, J. Floros, M.A. Gimbrone Jr., E. Hoffman, R.D. Hubmayr, M. Leppert, S. Matalon, R. Munford, P. Parsons, A.S. Slutsky, K.J. Tracey, P. Ward, D.B. Gail, A.L. Harabin, Future research directions in acute lung injury: summary of a National Heart, Lung, and Blood Institute working group, Am. J. Respir. Crit. Care Med. 167 (7) (2003) 1027–1035.

[3] R.G. Brower, Mechanical ventilation in acute lung injury and ARDS, Tidal volume reduction, Critical care clinics 18 (1) (2002) 1–13, v.

[4] L.B. Ware, M.A. Matthay, The acute respiratory distress syndrome, N. Engl. J. Med. 342 (18) (2000) 1334–1349.

[5] ARDSNet, Ventilation with lower tidal volumes as compared with traditional tidal volumes for acute lung injury and the acute respiratory distress syndrome. The Acute Respiratory Distress Syndrome Network, N. Engl. J. Med. 342 (18) (2000) 1301–1308.

[6] O. Gajic, F. Frutos-Vivar, A. Esteban, R.D. Hubmayr, A. Anzueto, Ventilator settings as a risk factor for acute respiratory distress syndrome in mechanically ventilated patients, Intensive Care Med. 31 (7) (2005) 922–926.

[7] D.P. Carlton, J.J. Cummings, R.G. Scheerer, F.R. Poulain, R.D. Bland, Lung overexpansion increases pulmonary microvascular protein permeability in young lambs, J. Appl. Physiol. 69 (2) (1990) 577–583.

[8] D. Dreyfuss, G. Saumon, Ventilator-induced lung injury: lessons from experimental studies, Am. J. Respir. Crit. Care Med. 157 (1) (1998) 294–323.

[9] D. Dreyfuss, P. Soler, G. Basset, G. Saumon, High inflation pressure pulmonary edema. Respective effects of high airway pressure, high tidal volume, and positive end-expiratory pressure, Am. Rev. Respir. Dis. 137 (5) (1988) 1159–1164.

[10] J.C. Parker, L.A. Hernandez, G.L. Longenecker, K. Peevy, W. Johnson, Lung edema caused by high peak inspiratory pressures in dogs. Role of increased microvascular filtration pressure and permeability, Am. Rev. Respir. Dis. 142 (2) (1990) 321–328.

[11] J.C. Parker, L.A. Hernandez, K.J. Peevy, Mechanisms of ventilator-induced lung injury, Crit. Care Med. 21 (1) (1993) 131–143.

[12] H.H. Webb, D.F. Tierney, Experimental pulmonary edema due to intermittent positive pressure ventilation with high inflation pressures. Protection by positive end-expiratory pressure, Am. Rev. Respir. Dis. 110 (5) (1974) 556–565.

[13] S. Kumar, X. Sun, S.K. Noonepalle, Q. Lu, E. Zemskov, T. Wang, S. Aggarwal, C. Gross, S. Sharma, A.A. Desai, Y. Hou, S. Dasarathy, N. Qu, V. Reddy, S.G. Lee, M. Cherian-Shaw, J.X. Yuan, J.D. Catravas, R. Rafikov, J.G.N. Garcia, S.M. Black, Hyper-activation of pp60(Src) limits nitric oxide signaling by increasing asymmetric dimethylarginine levels during acute lung injury, Free Radic. Biol. Med. 102 (2017) 217–228.

[14] F. Chen, Y. Wang, R. Rafikov, S. Haigh, W.B. Zhi, S. Kumar, P.T. Doulias, O. Rafikova, H. Pillich, T. Chakraborty, R. Lucas, A.D. Verin, J.D. Catravas, J. X. She, S.M. Black, D.J.R. Fulton, RhoA S-nitrosylation as a regulatory mechanism influencing endothelial barrier function in response to G(+)-bacterial toxins, Biochem. Pharmacol. 127 (2017) 34–45.

[15] A. Di, D. Mehta, A.B. Malik, ROS-activated calcium signaling mechanisms regulating endothelial barrier function, Cell Calcium 60 (3) (2016) 163–171.

[16] N. Barabutis, A. Verin, J.D. Catravas, Regulation of pulmonary endothelial barrier function by kinases, Am. J. Physiol. Lung Cell Mol. Physiol. 311 (5) (2016) L832–L845.

[17] M. Kellner, S. Noonepalle, Q. Lu, A. Srivastava, E. Zemskov, S.M. Black, ROS signaling in the pathogenesis of acute lung injury (ALI) and acute respiratory distress syndrome (ARDS), Adv. Exp. Med. Biol. 967 (2017) 105–137.

[18] F. Chen, S. Kumar, Y. Yu, S. Aggarwal, C. Gross, Y. Wang, T. Chakraborty, A. D. Verin, J.D. Catravas, R. Lucas, S.M. Black, D.J. Fulton, PKC-dependent phosphorylation of eNOS at T495 regulates eNOS coupling and endothelial barrier function in response to G+ -toxins, PLoS One 9 (7) (2014), e99823.

[19] X. Sun, S. Kumar, S. Sharma, S. Aggarwal, Q. Lu, C. Gross, O. Rafikova, S.G. Lee, S. Dasarathy, Y. Hou, M.L. Meadows, W. Han, Y. Su, J.R. Fineman, S.M. Black, Endothelin-1 induces a glycolytic switch in pulmonary arterial endothelial cells via the mitochondrial translocation of endothelial nitric oxide synthase, Am. J. Respir. Cell Mol. Biol. 50 (6) (2014) 1084–1095.

[20] D.L. Cioffi, K. Lowe, D.F. Alvarez, C. Barry, T. Stevens, TRPing on the lung endothelium: calcium channels that regulate barrier function, Antioxidants Redox Signal. 11 (4) (2009) 765–776.

[21] D.F. Alvarez, J.A. King, D. Weber, E. Addison, W. Liedtke, M.I. Townsley, Transient receptor potential vanilloid 4-mediated disruption of the alveolar septal barrier: a novel mechanism of acute lung injury, Circ. Res. 99 (9) (2006) 988–995.

[22] N. Pairet, S. Mang, G. Fois, M. Keck, M. Kuhnbach, J. Gindele, M. Frick, P. Dietl, D. J. Lamb, TRPV4 inhibition attenuates stretch-induced inflammatory cellular responses and lung barrier dysfunction during mechanical ventilation, PLoS One 13 (4) (2018), e0196055.

[23] R.K. Adapala, P.K. Talasila, I.N. Bratz, D.X. Zhang, M. Suzuki, J.G. Meszaros, C. K. Thodeti, PKCalpha mediates acetylcholine-induced activation of TRPV4-dependent calcium influx in endothelial cells, Am. J. Physiol. Heart Circ. Physiol. 301 (3) (2011) H757–H765.

[24] L.K. Kelly, S. Wedgwood, R.H. Steinhorn, S.M. Black, Nitric oxide decreases endothelin-1 secretion through the activation of soluble guanylate cyclase, Am. J. Physiol. Lung Cell Mol. Physiol. 286 (5) (2004) L984–L991.

[25] M.A. Matthay, S. Bhattacharya, D. Gaver, L.B. Ware, L.H. Lim, O. Syrkina, F. Eyal, R. Hubmayr, Ventilator-induced lung injury: in vivo and in vitro mechanisms, Am. J. Physiol. Lung Cell Mol. Physiol. 283 (4) (2002) L678–L682.

[26] B. Emr, L.A. Gatto, S. Roy, J. Satalin, A. Ghosh, K. Snyder, P. Andrews, N. Habashi, W. Marx, L. Ge, G. Wang, D.A. Dean, Y. Vodovotz, G. Nieman, Airway pressure release ventilation prevents ventilator-induced lung injury in normal lungs, JAMA Surg 148 (11) (2013) 1005–1012.

[27] G. Grynkiewcz, M. Poenie, R.Y. Tsien, A new generation of Ca2+ indicators with greatly improved fluorescence properties, J. Biol. Chem. 260 (6) (1985) 3440–3450.

[28] S. Aggarwal, C.M. Gross, S. Kumar, S. Datar, P. Oishi, G. Kalkan, C. Schreiber, S. Fratz, J.R. Fineman, S.M. Black, Attenuated vasodilatation in lambs with endogenous and exogenous activation of cGMP signaling: role of protein kinase G nitration, J. Cell. Physiol. 226 (12) (2011) 3104–3113.

[29] W. Casavan, Y. Gaidoukevitch, Colocalization of fluorescent probes using image-pro® Plus v. 5.0, Microscopy Today 11 (6) (2003) 48–50.

[30] J.N. Gonzales, K.M. Kim, M.A. Zemskova, R. Rafikov, B. Heeke, M.N. Varn, S. Black, T.P. Kennedy, E.A. Zemskov, Low anticoagulant heparin blocks thrombin-induced endothelial permeability in a PAR-dependent manner, Vasc. Pharmacol. 62 (2) (2014) 63–71.

[31] S. Aggarwal, C.M. Gross, S. Kumar, C. Dimitropoulou, S. Sharma, B.A. Gorshkov, S. Sridhar, Q. Lu, N.V. Bogatcheva, A.J. Jezierska-Drutel, R. Lucas, A.D. Verin, J. D. Catravas, S.M. Black, Dimethylarginine dimethylaminohydrolase II overexpression attenuates LPS-mediated lung leak in acute lung injury, Am. J. Respir. Cell Mol. Biol. 50 (3) (2014) 614–625.

[32] International consensus conferences in intensive care medicine, Ventilator-associated lung injury in ARDS. This official conference report was cosponsored by the American thoracic society, the European society of intensive Care medicine, and the societe de Reanimation de Langue francaise, and was approved by the ATS board of directors, july 1999, Am. J. Respir. Crit. Care Med. 160 (6) (1999) 2118–2124.

[33] O. Gajic, S.I. Dara, J.L. Mendez, A.O. Adesanya, E. Festic, S.M. Caples, R. Rana, J. L. St Sauver, J.F. Lymp, B. Afessa, R.D. Hubmayr, Ventilator-associated lung injury in patients without acute lung injury at the onset of mechanical ventilation, Crit. Care Med. 32 (9) (2004) 1817–1824.

[34] R.M. Determann, A. Royakkers, E.K. Wolthuis, A.P. Vlaar, G. Choi, F. Paulus, J. J. Hofstra, M.J. de Graaff, J.C. Korevaar, M.J. Schultz, Ventilation with lower tidal volumes as compared with conventional tidal volumes for patients without acute lung injury: a preventive randomized controlled trial, Crit. Care 14 (1) (2010) R1.

[35] A.S. Slutsky, Basic science in ventilator-induced lung injury: implications for the bedside, Am. J. Respir. Crit. Care Med. 163 (3 Pt 1) (2001) 599–600.

[36] Ventilation with lower tidal volumes as compared with traditional tidal volumes for acute lung injury and the acute respiratory distress syndrome. The Acute Respiratory Distress Syndrome Network, N. Engl. J. Med. 342 (18) (2000) 1301–1308.

[37] F.E. Curry, Modulation of venular microvessel permeability by calcium influx into endothelial cells, Faseb. J.: official publication of the Federation of American Societies for Experimental Biology 6 (7) (1992) 2456–2466.

[38] C. Tiruppathi, R.D. Minshall, B.C. Paria, S.M. Vogel, A.B. Malik, Role of Ca2+ signaling in the regulation of endothelial permeability, Vasc. Pharmacol. 39 (4-5) (2002) 173–185.

[39] M.G. Madej, C.M. Ziegler, Dawning of a new era in TRP channel structural biology by cryo-electron microscopy, Pflügers Archiv 470 (2) (2018) 213–225.

[40] T. Hof, S. Chaigne, A. Recalde, L. Salle, F. Brette, R. Guinamard, Transient receptor potential channels in cardiac health and disease, Nat. Rev. Cardiol. 16 (6) (2019) 344–360.

[41] J.P. White, M. Cibelli, L. Urban, B. Nilius, J.G. McGeown, I. Nagy, TRPV4: molecular conductor of a diverse orchestra, Physiol. Rev. 96 (3) (2016) 911–973.

[42] K. Venkatachalam, C. Montell, TRP channels, Annu. Rev. Biochem. 76 (2007) 387–417.

[43] K. Vaporidi, R.C. Francis, K.D. Bloch, W.M. Zapol, Nitric oxide synthase 3 contributes to ventilator-induced lung injury, Am. J. Physiol. Lung Cell Mol. Physiol. 299 (2) (2010) L150–L159.

[44] Z. Hu, Y. Xiong, X. Han, C. Geng, B. Jiang, Y. Huo, J. Luo, Acute mechanical stretch promotes eNOS activation in venous endothelial cells mainly via PKA and Akt pathways, PLoS One 8 (8) (2013), e71359.

[45] S. Wedgwood, C.J. Mitchell, J.R. Fineman, S.M. Black, Developmental differences in the shear stress-induced expression of endothelial NO synthase: changing role of AP-1, Am. J. Physiol. Lung Cell Mol. Physiol. 284 (4) (2003) L650–L662.

[46] S.M. Black, J.R. Fineman, R.H. Steinhorn, J. Bristow, S.J. Soifer, Increased endothelial NOS in lambs with increased pulmonary blood flow and pulmonary hypertension, Am. J. Physiol. 275 (5) (1998) H1643–H1651.

[47] S.M. Black, M.J. Johengen, Z.D. Ma, J. Bristow, S.J. Soifer, Ventilation and oxygenation induce endothelial nitric oxide synthase gene expression in the lungs of fetal lambs, J. Clin. Invest. 100 (6) (1997) 1448–1458.

[48] S.A. Kim, J.Y. Sung, C.H. Woo, H.C. Choi, Laminar shear stress suppresses vascular smooth muscle cell proliferation through nitric oxide-AMPK pathway, Biochem. Biophys. Res. Commun. 490 (4) (2017) 1369–1374.

[49] K. Binti Md Isa, N. Kawasaki, K. Ueyama, T. Sumii, S. Kudo, Effects of cold exposure and shear stress on endothelial nitric oxide synthase activation, Biochem. Biophys. Res. Commun. 412 (2) (2011) 318–322.

[50] J. Tian, Y. Hou, Q. Lu, D.A. Wiseman, F. Vasconcelos Fonseca, S. Elms, D.J. Fulton, S.M. Black, A novel role for caveolin-1 in regulating endothelial nitric oxide synthase activation in response to H2O2 and shear stress, Free Radic. Biol. Med. 49 (2) (2010) 159–170.

[51] G.K. Kolluru, S. Sinha, S. Majumder, A. Muley, J.H. Siamwala, R. Gupta, S. Chatterjee, Shear stress promotes nitric oxide production in endothelial cells by sub-cellular delocalization of eNOS: a basis for shear stress mediated angiogenesis, Nitric Oxide 22 (4) (2010) 304–315.

[52] S. Kumar, N. Sud, F.V. Fonseca, Y. Hou, S.M. Black, Shear stress stimulates nitric oxide signaling in pulmonary arterial endothelial cells via a reduction in catalase activity: role of protein kinase C delta, Am. J. Physiol. Lung Cell Mol. Physiol. 298 (1) (2010) L105–L116.

[53] K.L. Siu, L. Gao, H. Cai, Differential roles of protein complexes NOX1-NOXO1 and NOX2-p47phox in mediating endothelial redox responses to oscillatory and unidirectional laminar shear stress, J. Biol. Chem. 291 (16) (2016) 8653–8662.

[54] R. Sathanoori, P. Bryl-Gorecka, C.E. Muller, L. Erb, G.A. Weisman, B. Olde, D. Erlinge, P2Y2 receptor modulates shear stress-induced cell alignment and actin stress fibers in human umbilical vein endothelial cells, Cell. Mol. Life Sci. 74 (4) (2017) 731–746.

[55] S. Ghosh, M. Gupta, W. Xu, D.A. Mavrakis, A.J. Janocha, S.A. Comhair, M. M. Haque, D.J. Stuehr, J. Yu, P. Polgar, S.V. Naga Prasad, S.C. Erzurum, Phosphorylation inactivation of endothelial nitric oxide synthesis in pulmonary arterial hypertension, Am. J. Physiol. Lung Cell Mol. Physiol. 310 (11) (2016) L1199–L1205.

[56] M.Y. Jian, J.A. King, A.B. Al-Mehdi, W. Liedtke, M.I. Townsley, High vascular pressure-induced lung injury requires P450 epoxygenase-dependent activation of TRPV4, Am. J. Respir. Cell Mol. Biol. 38 (4) (2008) 386–392.

[57] K. Hamanaka, M.Y. Jian, D.S. Weber, D.F. Alvarez, M.I. Townsley, A.B. Al-Mehdi, J.A. King, W. Liedtke, J.C. Parker, TRPV4 initiates the acute calcium-dependent permeability increase during ventilator-induced lung injury in isolated mouse lungs, Am. J. Physiol. Lung Cell Mol. Physiol. 293 (4) (2007) L923–L932.

[58] C. Tiruppathi, M. Freichel, S.M. Vogel, B.C. Paria, D. Mehta, V. Flockerzi, A. B. Malik, Impairment of store-operated Ca2+ entry in TRPC4(-/-) mice interferes with increase in lung microvascular permeability, Circ. Res. 91 (1) (2002) 70–76.

[59] J. Yin, L. Michalick, C. Tang, A. Tabuchi, N. Goldenberg, Q. Dan, K. Awwad, L. Wang, L. Erfinanda, G. Nouailles, M. Witzenrath, A. Vogelzang, L. Lv, W.L. Lee, H. Zhang, O. Rotstein, A. Kapus, K. Szaszi, I. Fleming, W.B. Liedtke, H. Kuppe, W. M. Kuebler, Role of transient receptor potential vanilloid 4 in neutrophil activation and acute lung injury, Am. J. Respir. Cell Mol. Biol. 54 (3) (2016) 370–383.

[60] L. Gattinoni, M. Bombino, P. Pelosi, A. Lissoni, A. Pesenti, R. Fumagalli, M. Tagliabue, Lung structure and function in different stages of severe adult respiratory distress syndrome, J. Am. Med. Assoc. 271 (22) (1994) 1772–1779.

[61] C.M. Gross, R. Rafikov, S. Kumar, S. Aggarwal, P.B. Ham 3rd, M.L. Meadows, M. Cherian-Shaw, A. Kangath, S. Sridhar, R. Lucas, S.M. Black, Endothelial nitric oxide synthase deficient mice are protected from lipopolysaccharide induced acute lung injury, PloS One 10 (3) (2015), e0119918.

[62] K. Murakami, P. Enkhbaatar, Y.M. Yu, L.D. Traber, R.A. Cox, H.K. Hawkins, R. G. Tompkins, D. Herndon, D.L. Traber, L-arginine attenuates acute lung injury after smoke inhalation and burn injury in sheep, Shock 28 (4) (2007) 477–483.

[63] S. Sharma, A. Smith, S. Kumar, S. Aggarwal, I. Rehmani, C. Snead, C. Harmon, J. Fineman, D. Fulton, J.D. Catravas, S.M. Black, Mechanisms of nitric oxide synthase uncoupling in endotoxin-induced acute lung injury: role of asymmetric dimethylarginine, Vasc. Pharmacol. 52 (5-6) (2010) 182–190.

[64] U. Forstermann, W.C. Sessa, Nitric oxide synthases: regulation and function, Eur. Heart J. 33 (7) (2012) 829–837, 837a-837d.

[65] R. Rafikov, F.V. Fonseca, S. Kumar, D. Pardo, C. Darragh, S. Elms, D. Fulton, S. M. Black, eNOS activation and NO function: structural motifs responsible for the posttranslational control of endothelial nitric oxide synthase activity, J. Endocrinol. 210 (3) (2011) 271–284.

[66] M.J. Crabtree, K.M. Channon, Synthesis and recycling of tetrahydrobiopterin in endothelial function and vascular disease, Nitric Oxide 25 (2) (2011) 81–88.

[67] A.C. Grobe, S.M. Wells, E. Benavidez, P. Oishi, A. Azakie, J.R. Fineman, S.M. Black, Increased oxidative stress in lambs with increased pulmonary blood flow and pulmonary hypertension: role of NADPH oxidase and endothelial NO synthase, Am. J. Physiol. Lung Cell Mol. Physiol. 290 (5) (2006) L1069–L1077.

[68] R. Rafikov, O. Rafikova, S. Aggarwal, C. Gross, X. Sun, J. Desai, D. Fulton, S. M. Black, Asymmetric dimethylarginine induces endothelial nitric-oxide synthase mitochondrial redistribution through the nitration-mediated activation of Akt1, J. Biol. Chem. 288 (9) (2013) 6212–6226.

[69] J. Seo, D.H. Cho, H.J. Lee, M.S. Sung, J.Y. Lee, K.J. Won, J.H. Park, I. Jo, Citron Rho-interacting kinase mediates arsenite-induced decrease in endothelial nitric oxide synthase activity by increasing phosphorylation at threonine 497: mechanism underlying arsenite-induced vascular dysfunction, Free Radic. Biol. Med. 90 (2016) 133–144.

[70] F. Abedi, A.W. Hayes, R. Reiter, G. Karimi, Acute lung injury: the therapeutic role of Rho kinase inhibitors, Pharmacol. Res. 155 (2020) 104736.

[71] X. Sun, M. Kellner, A.A. Desai, T. Wang, Q. Lu, A. Kangath, N. Qu, C. Klinger, S. Fratz, J.X. Yuan, J.R. Jacobson, J.G. Garcia, R. Rafikov, J.R. Fineman, S. M. Black, Asymmetric dimethylarginine stimulates Akt1 phosphorylation via heat shock protein 70-facilitated carboxyl-terminal modulator protein degradation in pulmonary arterial endothelial cells, Am. J. Respir. Cell Mol. Biol. 55 (2) (2016) 275–287.

[72] T. Wang, C. Gross, A.A. Desai, E. Zemskov, X. Wu, A.N. Garcia, J.R. Jacobson, J. X. Yuan, J.G. Garcia, S.M. Black, Endothelial cell signaling and ventilator-induced lung injury: molecular mechanisms, genomic analyses, and therapeutic targets, Am. J. Physiol. Lung Cell Mol. Physiol. 312 (4) (2017) L452–L476.

[73] B.K. Davis, H. Wen, J.P. Ting, The inflammasome NLRs in immunity, inflammation, and associated diseases, Annu. Rev. Immunol. 29 (2011) 707–735.

[74] F. Martinon, K. Burns, J. Tschopp, The inflammasome: a molecular platform triggering activation of inflammatory caspases and processing of proIL-beta, Mol. Cell. 10 (2) (2002) 417–426.

[75] F.G. Bauernfeind, G. Horvath, A. Stutz, E.S. Alnemri, K. MacDonald, D. Speert, T. Fernandes-Alnemri, J. Wu, B.G. Monks, K.A. Fitzgerald, V. Hornung, E. Latz, Cutting edge: NF-kappaB activating pattern recognition and cytokine receptors license NLRP3 inflammasome activation by regulating NLRP3 expression, J. Immunol. 183 (2) (2009) 787–791.

[76] A. Abderrazak, T. Syrovets, D. Couchie, K. El Hadri, B. Friguet, T. Simmet, M. Rouis, NLRP3 inflammasome: from a danger signal sensor to a regulatory node of oxidative stress and inflammatory diseases, Redox Biol 4 (2015) 296–307.

[77] L. Martinez-Caro, N. Nin, C. Sanchez-Rodriguez, A. Ferruelo, M. El Assar, M. de Paula, P. Fernandez-Segoviano, A. Esteban, J.A. Lorente, Inhibition of nitro-oxidative stress attenuates pulmonary and systemic injury induced by high-tidal volume mechanical ventilation, Shock 44 (1) (2015) 36–43.

[78] L. Martinez-Caro, J.A. Lorente, J. Marin-Corral, C. Sanchez-Rodriguez, A. Sanchez-Ferrer, N. Nin, A. Ferruelo, M. de Paula, P. Fernandez-Segoviano, E. Barreiro, A. Esteban, Role of free radicals in vascular dysfunction induced by high tidal volume ventilation, Intensive Care Med. 35 (6) (2009) 1110–1119.

[79] H. Gunaydin, K.N. Houk, Mechanisms of peroxynitrite-mediated nitration of tyrosine, Chem. Res. Toxicol. 22 (5) (2009) 894–898.

[80] S. Sharma, N. Sud, D.A. Wiseman, A.L. Carter, S. Kumar, Y. Hou, T. Rau, J. Wilham, C. Harmon, P. Oishi, J.R. Fineman, S.M. Black, Altered carnitine homeostasis is associated with decreased mitochondrial function and altered nitric oxide signaling in lambs with pulmonary hypertension, Am. J. Physiol. Lung Cell Mol. Physiol. 294 (1) (2008) L46–L56.

[81] S. Sharma, A. Aramburo, R. Rafikov, X. Sun, S. Kumar, P.E. Oishi, S.A. Datar, G. Raff, K. Xoinis, G. Kalkan, S. Fratz, J.R. Fineman, S.M. Black, L-carnitine preserves endothelial function in a lamb model of increased pulmonary blood flow, Pediatr. Res. 74 (1) (2013) 39–47.

[82] S. Sharma, X. Sun, S. Agarwal, R. Rafikov, S. Dasarathy, S. Kumar, S.M. Black, Role of carnitine acetyl transferase in regulation of nitric oxide signaling in pulmonary arterial endothelial cells, Int. J. Mol. Sci. 14 (1) (2012) 255–272.

[83] X. Sun, S. Sharma, S. Fratz, S. Kumar, R. Rafikov, S. Aggarwal, O. Rafikova, Q. Lu, T. Burns, S. Dasarathy, J. Wright, C. Schreiber, M. Radman, J.R. Fineman, S. M. Black, Disruption of endothelial cell mitochondrial bioenergetics in lambs with increased pulmonary blood flow, Antioxidants Redox Signal. 18 (14) (2013) 1739–1752.

[84] S. Sharma, X. Sun, R. Rafikov, S. Kumar, Y. Hou, P.E. Oishi, S.A. Datar, G. Raff, J. R. Fineman, S.M. Black, PPAR-gamma regulates carnitine homeostasis and mitochondrial function in a lamb model of increased pulmonary blood flow, PLoS One 7 (9) (2012), e41555.

[85] H. Cui, N. Xie, S. Banerjee, J. Ge, S. Guo, G. Liu, Impairment of fatty acid oxidation in alveolar epithelial cells mediates acute lung injury, Am. J. Respir. Cell Mol. Biol. 60 (2) (2019) 167–178.

[86] O. Kaya, Y.S. Koca, I. Barut, S. Baspinar, M.Z. Sabuncuoglu, L-carnitine reduces acute lung injury in experimental biliary obstruction, Saudi Med. J. 36 (9) (2015) 1046–1052.

[87] M.M. Sayed-Ahmed, H.H. Mansour, O.A. Gharib, H.F. Hafez, Acetyl-L-carnitine modulates bleomycin-induced oxidative stress and energy depletion in lung tissues, J. Egypt. Natl. Canc. Inst. 16 (4) (2004) 237–243.